UKRAINIAN JOURNAL OF MECHANICAL ENGINEERING AND MATERIALS SCIENCE
Vol. 8, No 1, 2022

Valentyna Vavrukh

Department of Materials Science and Engineering, Lviv Polytechnic National University,
12, S. Bandery Str., Lviv, Ukraine, e-mail: valentyna.i.vavrukh@lpnu.ua, ORCID 0000-0002-3143-2522

EFFECTS OF THE YTTRIA CONTENT AND SINTERING TEMPERATURE ON THE PHASE EVOLUTION IN YTTRIA-STABILIZED ZIRCONIA

Received: January 26, 2022 / Revised: March 14, 2022 / Accepted: March 30, 2022

https://doi.org/10.23939/ujmems2022.01.012

Abstract. The microstructure of YSZ ceramics stabilized by the various amount of yttria, namely 3 mol % Y_2O_3 (3YSZ), 4 mol% Y_2O_3 (4YSZ) and 5 mol % Y_2O_3 (5YSZ) has been studied. Three sintering temperatures, namely 1450 °C, 1500 °C and 1550 °C were used for each series of samples (3YSZ, 4YSZ, 5YSZ). The total area of the monoclinic and cubic zirconia phases in the microstructure of ceramics and the regularities of distribution of these phases were determined by ImageJ. Peculiarities of changes in volume percentage of the monoclinic and cubic phases with an increase in sintering temperature of ceramics were found. Quantitative analysis of these phases was carried out. The total distribution of the monoclinic and cubic phases by ranges of their areas was presented. Correlations between the yttria content, the sintering temperature and changes in the microstructure and phase balance of the studied ceramics were found.

Keywords: YSZ ceramics, microstructure, agglomerates of (cubic+monoclinic)-phases, sintering temperature.

Introduction and problem statement

Due to the unique combination of properties, zirconia ceramics are widely used in mechanical engineering, electronics, energy, chemistry, medicine, etc. These ceramics are used in gas turbine engines (thermal barrier coating of turbine blades, coating of the inner surface of the boiler chamber walls, coating of the gas turbine combustion chamber) [1–3], for heat-resistant lining of furnaces [4, 5], for fuel cells [6–8], electrodes [9], gas sensors [10], as a protective coating for alloys [11, 12], as a material for dental implants, dental prostheses, artificial bone endoprostheses [13–18]. Widespread use of zirconia ceramics is due to their low thermal conductivity, high strength, wear resistance, high fracture toughness, high corrosion resistance, biological inertness, and high biocompatibility. Properties of zirconia ceramics are determined by their microstructure and phase composition.

The main structural component of zirconia ceramic is zirconium dioxide. According to the phase diagram, zirconium dioxide exists in three crystallographic phases: monoclinic, tetragonal and cubic. There is a monoclinic phase in the structure of zirconia ceramic at 20 °C and atmospheric pressure. The monoclinic phase exists below 1127 °C, tetragonal between 1127 °C and 2370 °C, and cubic above 2370 °C [1]. The monoclinic phase is stable and the tetragonal phase is metastable, due to the phase transition of the tetragonal phase to the monoclinic phase and an increase in volume by 3–5 %. Doping of zirconia ceramic causes changes in the phase transitions temperature, which leads to stabilization at 20 °C not only monoclinic, but also tetragonal and cubic phases. Tetragonal and cubic phases stabilization in the structure of zirconia ceramic was carried out by its doping with oxides of yttrium [1, 19–23], aluminum [24], calcium [25], magnesium [5, 26], cerium [27–30], and titanium [2].

Doping zirconia ceramic allows to obtain and to stabilize the tetragonal phase at room temperature, the presence of which provides the unique properties of this ceramic. Doping additives, namely, their nature and concentration, as well as the grain size significantly affect the microstructure of ceramic and determine its stability [19].

Zirconia ceramic stabilized by 3 mol% Y_2O_3 characterized by high strength (about 700 MPa) and fracture toughness (K_c = 6–9 $MN \cdot m^{-3/2}$) due to the presence in its structure of fine-grained metastable tetragonal phase [20]. The reason for the high fracture toughness of this material was the martensitic transformation of the tetragonal phase grains into monoclinic (t→m) during deformation. This transformation accompanied by the absorption of deformation energy. In the structure of zirconia ceramic stabilized by 3 mol % Y_2O_3 there were three phases, namely tetragonal, monoclinic and cubic [22]. The relatively low strength and fracture toughness were due to the high content of the monoclinic phase (37.8 %). The disadvantage of this ceramic was the phase transformation (t→m), which accompanied by an expansion of the volume to 5 % and caused the formation of cracks during cooling.

Properties degradation of zirconia ceramic stabilized by 3 mol % Y_2O_3 under aging in water vapor conditions occurred due to the transformation of the tetragonal phase into monoclinic one [21]. It was concluded that the optimal sintering temperature for this ceramic is 1550 °C, at which the maximum microhardness (11.135 GPa) and high relative density (96.64 %) were achieved [23].

Doping additives and the grain size influenced the stability of the tetragonal phase under conditions of low-temperature degradation. The grain size of zirconia ceramic stabilized by 3 mol % Y_2O_3 after sintering at temperatures of 1350 °C and 1400 °C was less than 3 μm. Aluminum oxide and cerium oxide stabilized the grain size and increased the tetragonal phase stability. Therefore, no tetragonal to monoclinic phase transformation under aging in water vapor conditions occurred [19].

Zirconia ceramics microstructure and properties largely depend on the sintering temperature [19]. Therefore, ensuring the choice of optimal sintering mode of ceramics will allow obtaining a material with improved microstructure and, accordingly, properties.

Additional TiO_2 doping of zirconia ceramic stabilized by 7.6 % ± 1 % $YO_{1.5}$ significantly increased toughness by increasing the tetragonal phase stability [2]. This ceramic can be a promising material for thermal barrier coatings in gas turbine engines, because such growth of the toughness and phase stability significantly influence its strain tolerance, cyclic durability and erosion resistance. The microstructure and phase composition of zirconia ceramics are decisive in the formation of these properties.

Zirconia ceramic stabilized by 3 mol % Y_2O_3 was further doped with Al_2O_3 in order to increase the corrosion resistance in a humid environment at 150–250 °C. Even a small content of alloying additive (0.25 wt % Al_2O_3) increased the resistance to degradation of the ceramic surface, especially under water or water vapor conditions [24].

Zirconia ceramic doped by 8–10 mol % MgO contains tetragonal (t-ZrO_2), monoclinic (m-ZrO_2) and cubic phases (c-ZrO_2). This ceramic is characterized by high fracture toughness (8-15 $MPa \cdot m^{1/2}$), high bending strength (700 MPa) and high thermal shock resistance [26].

When co-alloying zirconia ceramic by 2.5 wt % Y_2O_3 and 25 wt % CeO_2, the cubic phase was observed in the structure in addition to the fully stabilized tetragonal phase. The presence of the cubic phase was explained by additional doping with cerium oxide [29]. Due to this phase composition, the thermophysical characteristics of such ceramic significantly improved, in particular high thermal shock resistance.

Doping and the optimal sintering modes of zirconia ceramic are determining factors for obtaining the desired structure and phase composition and, thus, improving the properties of such ceramic.

Main Material Presentation

ZrO_2 ceramics partially stabilized by 3, 4 and 5 mol % Y_2O_3 (3YSZ, 4YSZ, 5YSZ) have been studied. ZrO_2 powders with initial particle sizes of 100–150 nm and Y_2O_3 powders with initial particle sizes of 10–30 nm were used as raw materials for the production of such ceramics. The powders were mixed in appropriate proportions in a drum mill with the addition of isopropyl alcohol. From the resulting mixture of ZrO_2 and Y_2O_3 powders, a suspension by adding ethyl cellulose (polymer bond), dibutyl phthalate (plasticizer), isopropyl alcohol (solvent) was made. Then, until cessation of weight loss, the powder mixture was dried in an oven at 120 °C to remove residual liquid. The procedure of calcination of powders at 700 °C to obtain a specific distribution of particles size and phase composition was performed. To increase the density of the resulting mixture of powders, 5 % wt % polyvinyl butyral (5 % alcohol solution) was added [31–33]. Prismatic samples with a size of 4×4×50 mm were formed by the method of bilateral densification in metal form under a pressure of 50 MPa. The obtained prismatic samples were sintered in an electric resistance furnace for 2 h in argon, using conventional sintering techniques. Three sintering temperatures, namely 1450 °C, 1500 °C and 1550 °C were used for each series of samples (3YSZ, 4YSZ, 5YSZ) [21].

The microstructure was examined using an optical microscope MICROTECH MMT-14C at magnifications of 100 and 400 times. To conduct microstructural studies, the surface of the samples was ground, polished and etched in hydrofluoric acid for 15 min.

Analysis of microstructure was performed using specialized ImageJ software. The software was used to scale the image, manipulate the contrast of the image, sharpen, smooth, and detect boundaries. The total area of monoclinic and cubic phases in the microstructure and the area of the microstructural (c+m)-phase agglomerates have been determined by ImageJ. Firstly, we have set the spatial scale of the photo, selected the working area and analyzed the working area according to the set parameter, i.e. cross-sectional area. When using the function “Threshold”, microstructural components displayed in dark gray and the background displayed in white. This function set the lower and upper thresholds to segment the desired area and image background. Using the function “Set Measurements”, it was selected the parameters (data) to be analyzed by the software, particularly the cross-sectional area of the particles. Then, using the function “Analyze particles”, the required parameters were selected, namely

– in the field “Circularity”, the range from 0 (straight line) to 1.00 (circle) was set, in order to the software considered particles of any shape;

– the options were set for displaying the results (Display results) and summing the cross-sectional areas of all particles (Summarise).

As a result of the analysis by ImageJ software, the values of the total area of analyzed particles, the cross-sectional area of each particle, and the number of particles in the set ranges of their areas (0–20, 20–40, 40–60, 60–80, 80–100, 100–120, 120–140, 140–160, 160–180, 180–200, 200–220, 120–140, and 240–260 μm^2) were obtained.

Results and Discussion

Studies of the microstructure of 3YSZ, 4YSZ, and 5YSZ ceramics [21] have revealed the presence of the tetragonal, monoclinic and cubic phases in them. Monoclinic and cubic phases were of dark-gray color; therefore, they were easily identified in the images (Fig. 1). The tetragonal phase was of light-gray color; therefore, it was not identified in the images.

The measurement results are presented in graphs (Fig. 2), which exhibit the evolution of volume percentage (vol %) of the monoclinic and cubic phases in total for studied materials depending on the sintering temperature. The main peculiarities of the volume percentage changes of monoclinic and cubic phases with increase in sintering temperature of ceramics are clearly demonstrated at a high magnification (x400, Fig. 2, *a*), whereas quantitative analysis is better demonstrated at a low magnification (x100, Fig. 2, *b*).

It was found that with a more intensive increase of the monoclinic phase weight percentage (wt %), the volume percentage (vol %) growth of the monoclinic and cubic phases in total is suppressed. Conversely, when an increase in the monoclinic phase weight percentage decelerates, this process is intensified (Fig. 2, *a* and Fig. 3).

Besides, the evolution of volume percentage of the monoclinic and cubic phases depends on: 1) the yttria content (an increase in the volume percentage of monoclinic and cubic phases is intensified due to the yttria content growth); 2) the sintering temperature (an increase in the volume percentage of monoclinic and cubic phases is suppressed due to the sintering temperature growth). This is observed from the correlation between the (c+m)-phase weight percentage and the volume percentage of the monoclinic and cubic phases in total (Fig. 4).

For each material series (3YSZ, 4YSZ, and 5YSZ), the point in Fig. 4 was chosen that corresponds to the highest fracture toughness [21]. Then, mathematical function, that has the best fit to this point series, was obtained (dashed green line in Fig. 4) using Microsoft Excel curve fitting tools. The corresponding equation is as follows: $[(c+m)(vol\ \%)]=8\cdot 10^{-9}[(c+m)(wt\ \%)]^{5,9717}$. Thus, the volume percentage of (c+m)-phases must change according to this nonlinear law in order to achieve the maximum fracture toughness of the studied ceramic compositions. Positions of the points corresponding to the fitted curve are shown in Fig. 4: 3YSZ–1550, 4YSZ–1500, and 5YSZ–1450.

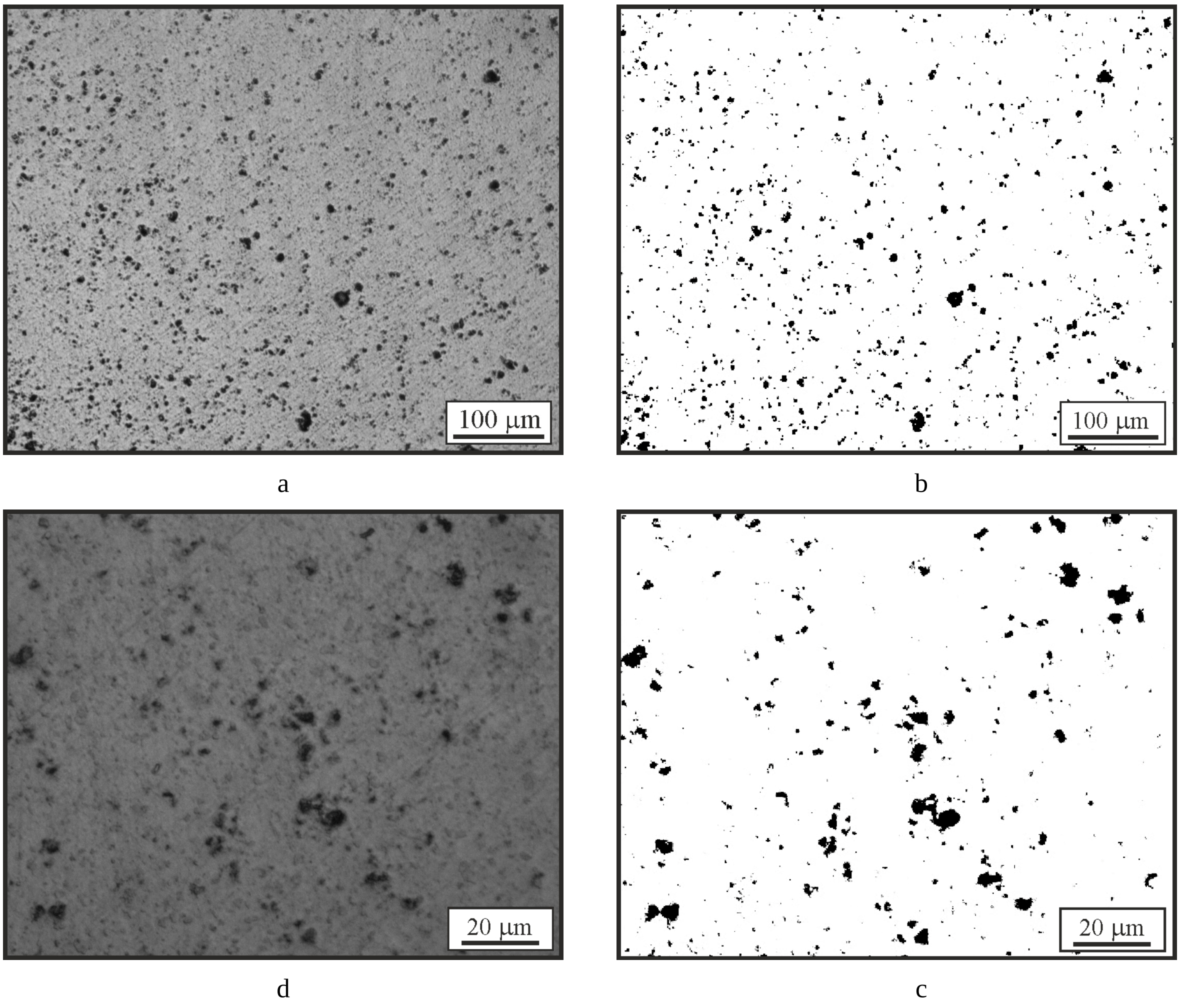

Fig. 1. Optical microstructure of 3YSZ ceramics sintered at 1450 °C (a, c) and after processing by the software ImageJ (b, d): magnification x100 (a, b); magnification x400 (c, d).

The distribution of the measured areas of the monoclinic and cubic phases (in total) by the ranges of their areas at magnifications x100 (Fig. 5, *a*) and x400 (Fig. 5, *b*) was also presented. It was found that the materials of 4YSZ series are characterized by the maximum number of (c+m)-phase agglomerates in the middle ranges of their areas (0–20, 20–40, 40–60, 60–80, 80–100 and 100–120 μm^2) as compared to other material variants.

This difference is especially noticeable for variant 4YSZ–1550, which correlates with the atypical ratio between the weight percentages of the monoclinic phase and the total weight percentages of the monoclinic and cubic phases as compared to other material variants (Fig. 3). In particular, at magnification x100 (Fig. 5, *a*), the following numbers of the (c+m)-phase agglomerates were recorded: 12253 agglomerates corresponding the range of area distribution of 0–20 μm^2, 344 agglomerates for the range 20–40 μm^2, 94 agglomerates for the range 40–60 μm^2, 45 agglomerates for the range 60–80 μm^2, 29 agglomerates for the range 80–100 μm^2, and 12 agglomerates for the range 100–120 μm^2. At magnification x400 (Fig. 5, *b*), a slightly different quantitative distribution was recorded, namely, 273328 agglomerates for the range 0–20 μm^2, 432 agglomerates for the range 20–40 μm^2, 64 agglomerates for the range 40–60 μm^2, and 16 agglomerates for the range 60–80 μm^2.

For this variant, the numbers of (c+m)-phase agglomerates are also consistent with the atypical deviation of the dependence between the weight percentage of (c+m)-phases and the volume percentage of monoclinic and cubic phases in total from the general tendency found for other studied material variants (Fig. 4).

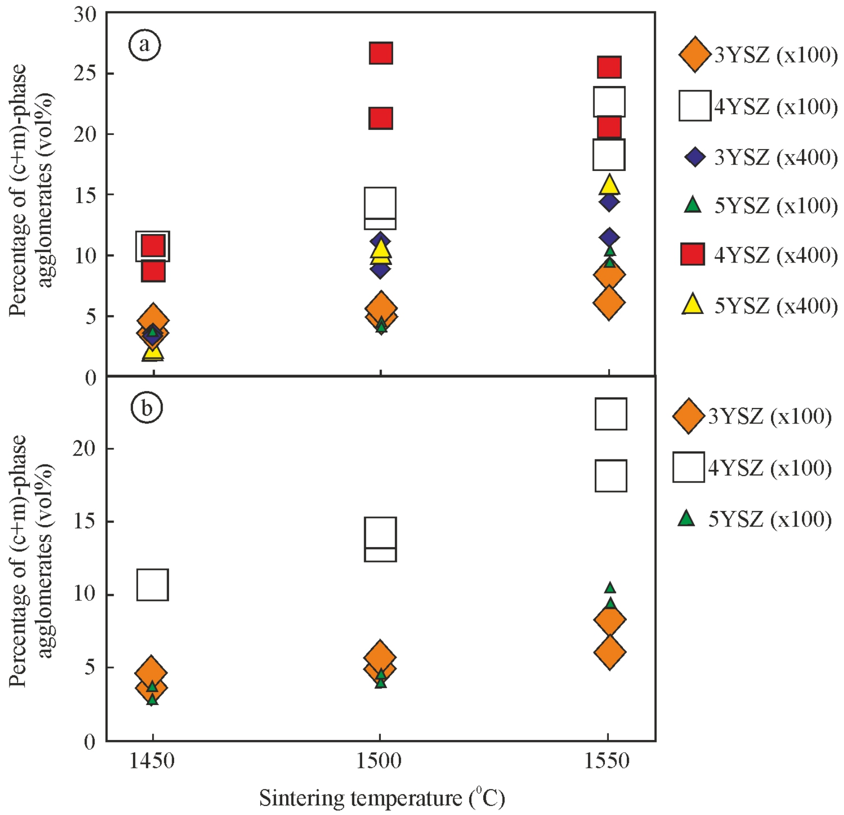

Fig. 2. Dependences of volume percentage of (c+m)-phase agglomerates on sintering temperature for studied materials. The number of agglomerates of (c+m)-phases was obtained after processing in the ImageJ software at magnifications x100 and x400 (a) and x100 (b)

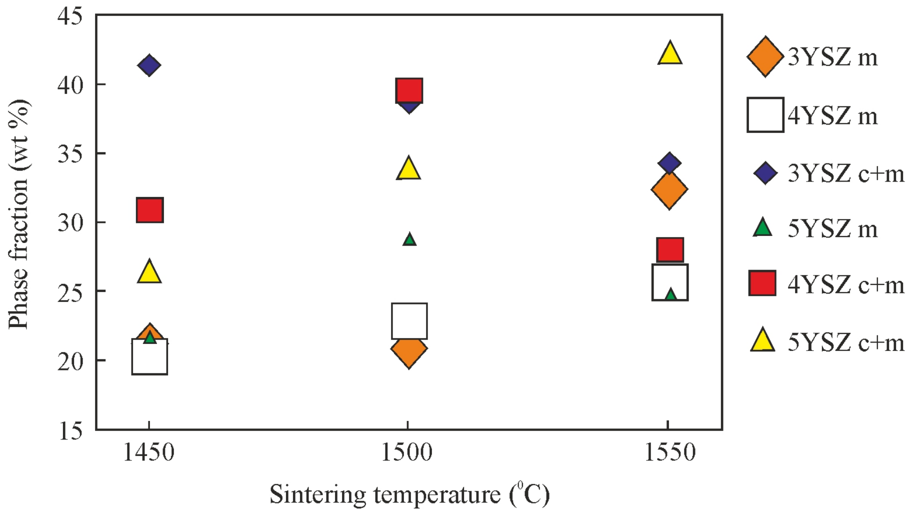

Fig. 3. Dependences of the monoclinic phase weight percentage and weight percentage of of (c+m)-phase agglomerates on sintering temperature for studied materials.

The lowest number of (c+m)-phase agglomerates in the middle ranges of their areas (20–40, 40–60, 60–80 and 80–100 μm^2) was found for the 5YSZ series, namely, variants 5YSZ–1450 and 5YSZ–1500 (Fig. 5, *a*, Fig. 5, *b*). This characteristic area distribution of the monoclinic and cubic phases is consistent with the high fracture toughness of variant 5YSZ–1450 [21], and variant 5YSZ–1500 is adjacent to it.

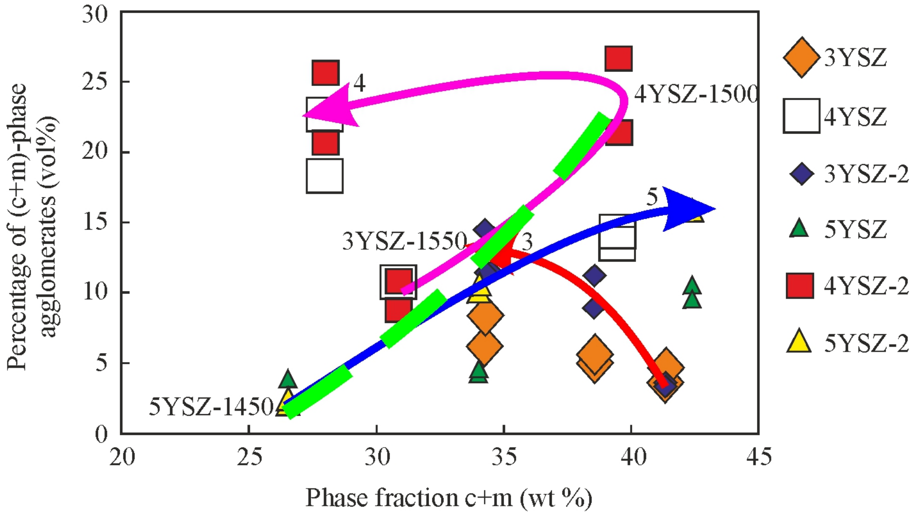

Fig. 4. Dependences of volume percentage of (c+m)-phase agglomerates on weight percentage of (c+m)-phases for studied materials. The arrows indicate directions of data evolution with increasing the sintering temperature.

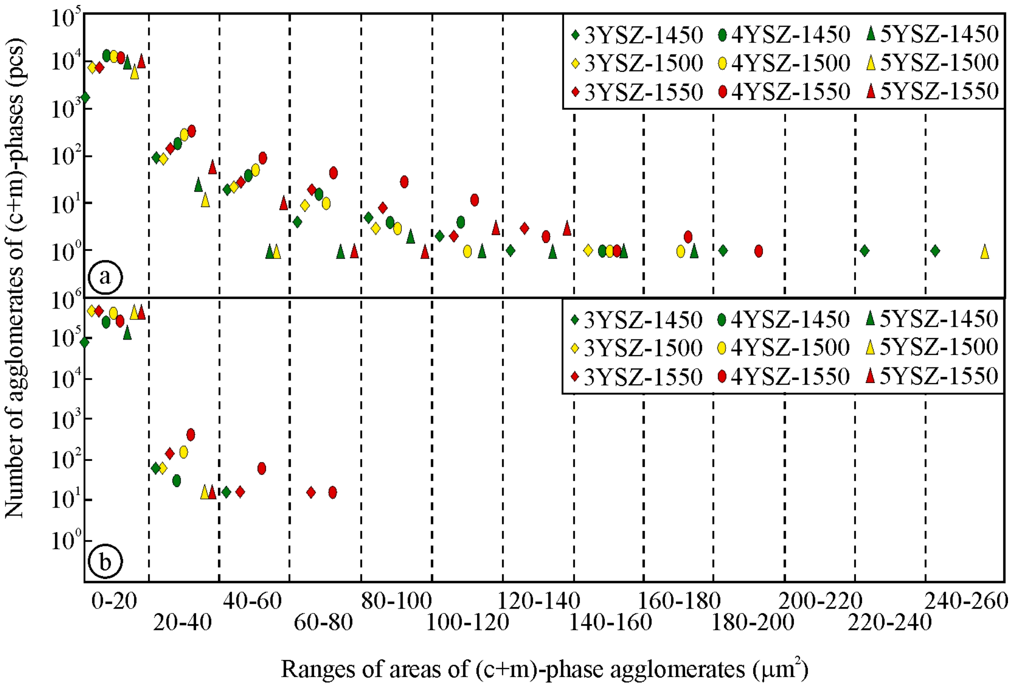

Fig. 5. Dependences of numbers of (c+m)-phase agglomerates on ranges of their areas, obtained after processing by ImageJ software at magnifications x100 (a) and x400 (b).

Quite low number of (c+m)-phase agglomerates in the middle ranges of their areas (0–20, 20–40, 40–60 and 60–80 μm^2) was also found for variant 3YSZ–1450, that can be explained by the insufficient sintering ability of 3YSZ ceramic and low intensity of phase transformations at 1450 °C.

In general, material variants exhibit the maximum number of (c+m)-phase agglomerates in the range of the smallest areas (0–20 μm^2), but in the middle ranges of their areas (20–40, 40–60, 60–80, 80–100 and 100–120 μm^2) the number of (c+m)-phase agglomerates is much smaller.

Conclusions

It was found that with a more intensive increase of the monoclinic phase weight percentage, the volume percentage growth of the monoclinic and cubic phases in total is suppressed. Conversely, when an increase in the monoclinic phase weight percentage decelerates, this process is intensified.

It was shown that the evolution of volume percentage of the monoclinic and cubic phases depends on the yttria content and sintering temperature. An increase in the volume percentage of monoclinic and cubic phases is intensified due to the yttria content growth, whereas it is suppressed due to the sintering temperature growth.

It was found that the materials of zirconia ceramic series stabilized by 4 mol% Y_2O_3 are characterized by the maximum number of (c+m)-phase agglomerates in the middle ranges of their areas (0–20, 20–40, 40–60, 60–80, 80–100 and 100–120 μm^2) as compared to other material variants. The lowest number of (c+m)-phase agglomerates in the middle ranges of their areas (20–40, 40–60, 60–80 and 80–100 μm^2) was found for zirconia ceramic series stabilized by 5 mol% Y_2O_3, obtained at sintering temperatures of 1450 °C (5YSZ–1450) and 1500 °C (5YSZ–1500). This characteristic area distribution of the monoclinic and cubic phases is consistent with the high fracture toughness of variant 5YSZ–1450.

Acknowledgements

This research was supported by the Ministry of Education and Science of Ukraine under the project number 0122U000952 “Development of a scientific basis for the creation of multifunctional oxide ceramic materials and coatings”.

References

[1] Sh. Jiang, X. Huang, Zh. He, A. Buyers, “Phase transformation and lattice parameter changes of non-trivalent rare earth-doped YSZ as a function of temperature”, *Journal of Materials Engineering and Performance*, vol. 27, pp. 2263–2270, 2018. https://doi.org/10.1007/s11665-018-3159-3.

[2] T. A. Schaedler, R. M. Leckie, S. Kra¨mer, A. G. Evans, C. G. Levi, “Toughening of nontransformable t’-YSZ by addition of titania”, *Journal of the American Ceramic Society*, vol. 90, no. 12, pp. 3896–3901, 2007.

[3] M. Zhao, W. Pan, Ch. Wan, Zh. Qu, Zh. Li, J. Yang, “Defect engineering in development of low thermal conductivity materials: A review”, *Journal of the European Ceramic Society*, vol. 37, no. 1, pp. 1–13, 2016. https://doi.org/10.1016/j.jeurceramsoc.2016.07.036.

[4] Y. Du, Zh. Jin, P. Huang, “Thermodynamic assessment of the ZrO_2-$YO_{1,5}$ system”, *Journal of the American Ceramic Society*, vol. 74, no. 7, pp. 1569–1577, 1991. https://doi.org/10.1111/j.1151-2916.1991.tb07142.x.

[5] C. Baudín, P. Pena, “The main role of the ZrO_2–MgO–CaO and ZrO_2–MgO–CaO–SiO_2 systems in the field of refractories”, *Boletín de la Sociedad Española de Cerámica y Vidrio*, 2021. https://doi.org/10.1016/j.bsecv.2021.09.009.

[6] B. Vasyliv, J. Milewski, V. Podhurska, T. Wejrzanowski, V. Kulyk, J. Skibiński, V. Vira, Ł. Szabłowski, A. Szczęśniak, O. Dybiński, “Study of the degradation of a fine-grained YSZ–NiO anode material during reduction in hydrogen and reoxidation in air”, *Applied Nanoscience*, vol. 12, pp. 965–975, 2022. https://doi.org/10.1007/s13204-021-01768-w.

[7] V. V. Kulyk, B. D. Vasyliv, Z. A. Duriagina, T. M. Kovbasiuk, I. A. Lemishka, “The effect of water vapor containing hydrogenous atmospheres on the microstructure and tendency to brittle fracture of anode materials of YSZ–NiO (Ni) system”, *Archives of Materials Science and Engineering*, vol. 108, no. 2, pp. 49–67, 2021. https://doi.org/10.5604/01.3001.0015.0254.

[8] B. Vasyliv, V. Kulyk, Z. Duriagina, D. Mierzwinski, T. Kovbasiuk, T. Tepla, “Estimation of the effect of redox treatment on microstructure and tendency to brittle fracture of anode materials of YSZ–NiO (Ni) system”, *Eastern-European Journal of Enterprise Technologies*, vol. 6, no. 12(108), pp. 61–71, 2020.

[9] A. J. Santos, S. Garcia-Segura, S. Dosta, I. G. Cano, C. A. Martínez-Huitle, E. Brillas, “A ceramic electrode of ZrO_2-Y_2O_3 for the generation of oxidant species in anodic oxidation. Assessment of the treatment of Acid Blue 29 dye in sulfate and chloride media”, *Separation and Purification Technology*, vol. 228, pp. 115747, 2019. https://doi.org/10.1016/j.seppur.2019.115747.

[10] Y. Yan, Z. Ma, J. Sun, M. Bu, Y. Huo, Z. Wang, Y. Li, N. Hu, “Surface microstructure-controlled ZrO_2 for highly sensitive room-temperature NO_2 sensors”, *Nano Materials Science*, vol. 3, no. 3, pp. 268–275, 2021.

[11] D. Kunying, Ch. Taotao, H. Zhiyong, “Formation and properties of porous ZrO_2-8wt%Y_2O_3 coatings”, *Rare Metal Materials and Engineering*, vol. 47, no. 6, pp. 1677–1681, 2018. https://doi.org/10.1016/S1875-5372(18)30149-8.

[12] B. Istrate, J. V. Rau, C. Munteanu, I. V. Antoniac, V. Saceleanu, “Properties and in vitro assessment of ZrO_2-based coatings obtained by atmospheric plasma jet spraying on biodegradable Mg-Ca and Mg-Ca-Zr alloys”, *Ceramics International*, vol. 46, no. 10, part B, pp. 15897–15906, 2020.

[13] F. Zarone, M.I. Mauro, G. Spagnuolo, E. Gherlone, R. Sorrentino, “Fourteen-year evaluation of posterior zirconia-based three-unit fixed dental prostheses: A prospective clinical study of all ceramic prosthesis”, *Journal of Dentistry*, vol. 101, pp. 103419, 2020. https://doi.org/10.1016/j.jdent.2020.103419.

[14] N. Antolino, C. Muhlstein, G. Hayes, J. Adair, R. Bermejo, "Strength limits in mesoscaled 3Y-TZP ceramics for micro-surgical instruments", *Journal of the Mechanical Behavior of Biomedical Materials,* vol. 91, pp. 99–108, 2019. https://doi.org/10.1016/j.jmbbm.2018.12.001.

[15] Ch. Li, F. Ai, X. Miao, H. Liao, F. Li, M. Liu, F. Yu, L. Dong, T. Li, X. Wang, "The return of ceramic implants": Rose stem inspired dual layered modification of ceramic scaffolds with improved mechanical and anti-infective properties", *Materials Science & Engineering C*, vol. 93, pp. 873–879, 2018.

[16] Ch. Liu, A. Eser, Th. Albrecht, V. Stournari, M. Felder, S. Heintze, Ch. Broeckmann, "Strength characterization and lifetime prediction ofdental ceramic materials", *Dental Materials*, vol. 37, no. 1, pp. 94–105, 2021. https://doi.org/10.1016/j.dental.2020.10.015.

[17] C. Santos, I. F. Coutinho, J. E. Amarante, M. F. Alves, M. M. Coutinho, C. R. Silva, "Mechanical properties of ceramic composites based on ZrO_2 co-stabilized by Y_2O_3–CeO_2 reinforced with Al_2O_3 platelets for dental implants", *Journal of the Mechanical Behavior of Biomedical Materials*, vol. 116, pp. 104372, 2021.

[18] Ch. Zhang, Zh. Jiang, L. Zhao, W. Guo, X. Gao, "Stability, rheological behaviors, and curing properties of 3Y–ZrO_2 and 3Y–ZrO_2/GO ceramic suspensions in stereolithography applied for dental implants", *Ceramics International*, vol. 47, pp. 13344–13350, 2021. https://doi.org/10.1016/j.ceramint.2021.01.191.

[19] L. Hallmann, P. Ulmer, E. Reusser, M. Louvel, Ch.H.F. Hämmerle, "Effect of dopants and sintering temperature on microstructure and low temperature degradation of dental Y-TZP-zirconia", *Journal of the European Ceramic Society*, vol. 32, pp. 4091–4104, 2012. https://doi.org/10.1016/j.jeurceramsoc.2012.07.032.

[20] T. K. Gupta, F. F. Lange, J. H. Bechtold, "Effect of stress-induced phase transformation on the properties of polycrystalline zirconia containing metastable tetragonal phase", Journal of Materials Science, vol. 13, pp. 1464–1470, 1978. https://doi.org/10.1007/BF00553200.

[21] V. V. Kulyk, Z. A. Duriagina, B. D. Vasyliv, V. I. Vavrukh, P. Ya. Lyutyy, T. M. Kovbasiuk, M. Ya. Holovchuk, "Effects of Yttria content and sintering temperature on the microstructure and tendency to brittle fracture of yttria-stabilized Zirconia", Archives of Materials Science and Engineering, vol. 109, no. 2, pp. 65–79, 2021.

[22] K. Wojteczko, Z. Pedzich, D. Zientara, K. Berent, K. Haberko, "Phenomena occurring upon the sintering of a mixture of yttria-zirconia nanometric powder and sub-micrometric pure zirconia powder", *Materials*, vol. 14, pp. 6937, 2021., https://doi.org/10.3390/ma14226937

[23] L. Ting, Ch. Weidong, J. Hongmin, Y. Shufang, M. Wen, "Characterization of YSZ ceramic nanopowders synthesized at different temperatures via polyacrylamide gel method", *Journal of Wuhan University of Technology-Mater. Sci. Ed.*, vol. 35, no. 3, 2020. https://doi.org/10.1007/s11595-020-2289-2.

[24] W. Pabst, J. Havrda, E. Gregorová, B. Krčmová, "Alumina toughened zirconia made by room temperature extrusion of ceramic pastes", *Ceramics – Silikáty*, vol. 44, no. 2, pp. 41–47, 2000.

[25] G. Chen, Y. Ling, Q. Li, H. Zheng, K. Li, Q. Jiang, J. Chen, M. Omran, L. Gao, "Crystal structure and thermomechanical properties of CaO-PSZ ceramics synthesised from fused ZrO_2", Ceramics International, vol. 46, pp. 15357–15363, 2020. https://doi.org/10.1016/j.ceramint.2020.03.079.

[26] J. A. B. Chaparro, A. R. Rojas, M. H. B. Bernal, A. A. Elguezabal, J. Echeberria, "Elucidating of the microstructure of ZrO_2 ceramics with additions of 1200°C heat treated ultrafine MgO powders: aging at 1420 °C", *Materials Chemistry and Physics*, vol. 106, pp. 45–53, 2007.

[27] M. Y. Smyrnova-Zamkova, O. V. Dudnik, O. I. Bykov, O. K. Ruban, O. I Khomenko, "Changes in the properties of ultrafine Al_2O_3–ZrO_2–Y_2O_3–CeO_2 powders after heat treatment in the range 400–1450 °C", *Powder Metallurgy and Metal Ceramics*, vol. 60, pp. 519–530, 2022.

[28] M. Y. Smyrnova-Zamkova, O. K. Ruban, O. I. Bykov, O. V. Dudnik, "Physico-chemical properties of fine-grained powder in Al_2O_3-ZrO_2 -Y_2O_3-CeO_2 system produced by combined method", *Composites Theory and Practice,* vol. 18, no. 4, pp. 234–240, 2018. https://doi.org/10.18524/2304-0947.2018.4(68).147820.

[29] M. Alfano, G. Di Girolamo, L. Pagnotta, D. Sun, "Processing, microstructure and mechanical properties of air plasma-sprayed ceria–yttria co-stabilized zirconia coatings", *Strain*, vol. 46, no. 5 (2), pp. 409–418, 2010.

[30] G. D. Girolamo, C. Blasi, M. Schioppa, L. Tapfer, "Structure and thermal properties of heat treated plasma sprayed ceria–yttria co-stabilized zirconia coatings", *Ceramics International*, vol. 36, no. 3, pp. 961–968, 2010.

[31] Y. Komatsu, A. Sciazko, N. Shikazono, "Isostatic pressing of screen printed nickel-gadolinium doped ceria anodes on electrolyte-supported solid oxide fuel cells", *Journal of Power Sources*, vol. 485, pp. 229317, 2021. https://doi.org/10.1016/j.jpowsour.2020.229317.

[32] B. Vasyliv, "Improvement of the electric conductivity of the material of anode in a fuel cell by the cyclic redox thermal treatment", *Materials Science*, vol. 46, no. 2, pp. 260–264, 2010.

[33] I. Danilenko, G. Lasko, I. Brykhanova, V. Burkhovetski, L. Ahkhozov, "The peculiarities of structure formation and properties of zirconia-based nanocomposites with addition of Al_2O_3 and NiO", *Nanoscale Research Letters*, vol. 12, no. 125, 2017. https://doi.org/10.1186/s11671-017-1901-7.